Multipath Fading Measurements at 5.8 GHz for Backscatter Tags With Multiple Antennas

Joshua D. Griffin, *Member, IEEE*, and Gregory D. Durgin, *Senior Member, IEEE*

***Abstract*—Multipath fading can be heavy for ultra-high frequency (UHF) and microwave backscatter radio systems used in applications such as radio frequency identification (RFID). This paper presents measurements of fading on the modulated signal backscattered from a transponder for backscatter radio systems that use multiple antennas at the interrogator and transponder. Measurements were performed at 5.8 GHz and estimates of the backscatter channel envelope distributions and fade margins were calculated. Results show that multipath fading can be reduced using multiple transponder antennas, bistatic interrogators with widely separated transmitter and receiver antennas, and conventional diversity combining at the interrogator receiver. The measured envelope distribution estimates are compared to previously derived distributions and show good agreement.**

***Index Terms*—Backscatter radio, diversity methods, fading channels, microwave radio propagation, multipath channels, probability, radio frequency identification, RFID.**

I. Introduction

BACKSCATTER radio systems are used extensively in applications such as radio frequency identification (RFID) and passive, wireless sensors because backscatter transponders, or *radio frequency (RF) tags*, can communicate while consuming very little power. In backscatter radio, the RF tag modulates the electromagnetic waves scattered from its antenna(s) by changing the reflection coefficient at the antenna's terminals. The signal that is scattered by the RF tag is supplied by an interrogator, or *reader*, and is detected by the reader's receiver.

Unfortunately, the reliability and range of backscatter radio is limited by several effects including multipath fading. To understand and combat multipath in backscatter radio systems, several researchers have reported measurements of both fading on the signal received by the RF tag and tag readability measurements [1]–[7]. Banerjee *et al.* [8] have presented spatial and frequency diversity measurements for the signal received by the RF tag at 915 MHz. In contrast, Kim *et al.* [9] have reported measured envelope cumulative distribution functions (CDFs) for the backscattered signal received from the RF tag at 2.4 GHz. Their measurements showed that multipath fading on the signal backscattered from the RF tag has different statistics than those encountered in conventional transmitter-to-receiver links [9]. This is because the backscatter channel is a spatial pinhole channel in which each RF tag antenna acts as a pinhole. While the pinholes increase fading on the modulated signal backscattered from the RF tag compared to a conventional transmitter-to-receiver link, adding additional pinholes can lessen their detrimental effect. This improvement is a *pinhole diversity* gain [10].

Another way to reduce fading in the backscatter channel is with conventional *antenna diversity*, which attempts to create multiple signals with uncorrelated fading using spatially-separated antennas at the reader. In general, if the signals are selected or coherently combined, fading on the output signal will be reduced. This technique was first introduced to backscatter radio by Ingram *et al.* [11] with fading simulations using both multiple reader and multiple RF tag antennas. Other researchers [12], [13] have used multiple antennas for this purpose at only the reader; however, none of these papers report multipath fading measurements for multi-antenna RF tags.

This paper details multipath fading measurements for RF tags with multiple antennas. Specifically, it expands previously reported non-line-of-sight (NLOS) fading measurements [14] to include LOS multipath fading measurements and conventional diversity combining results for both NLOS and LOS backscatter channels. Section II presents a multipath-fading distribution that applies to the modulated signal backscattered from the RF tag and Section III summarizes the previously discussed NLOS testbed and measurement setup [14], describes that for the LOS measurements, and provides details of backscatter radio signaling. Section IV summarizes the NLOS measurement results, presents the LOS fading measurements, and details diversity combining results in both the NLOS and LOS backscatter channels. Results are presented in terms of envelope distributions and fade margins. The Appendix provides a list of acronyms.

II. Backscatter Envelope Distributions

Multipath fading can be characterized by probability distributions and this paper references two distributions to describe fading observed on the backscattered signal from an RF tag. The first is the envelope distribution for the $M \times L \times N$ backscatter channel [10], [11]—i.e., the backscatter channel with M reader transmitter, L RF tag, and N reader receiver antennas—with Rayleigh-fading links. This distribution, which can take two forms depending on level of link correlation, has been discussed in detail previously [10] and will not be repeated here. The second is the envelope distribution of the $1 \times 1 \times 1$ backscatter

Manuscript received October 04, 2009; revised February 22, 2010; accepted March 20, 2010. Date of publication August 30, 2010; date of current version November 03, 2010. The work was supported in part by the National Science Foundation (NSF) CAREER Grant 0546955.

J. D. Griffin was with the ECE Department, Georgia Institute of Technology, Atlanta, GA 30332 USA. He is now with Disney Research, Pittsburgh, PA 15213 USA (e-mail: jdgriffin@ieee.org).

G. D. Durgin is with the ECE Department, Georgia Institute of Technology, Atlanta, GA 30332 USA (e-mail: durgin@ece.gatech.edu).

Color versions of one or more of the figures in this paper are available online at http://ieeexplore.ieee.org.

Digital Object Identifier 10.1109/TAP.2010.2071355

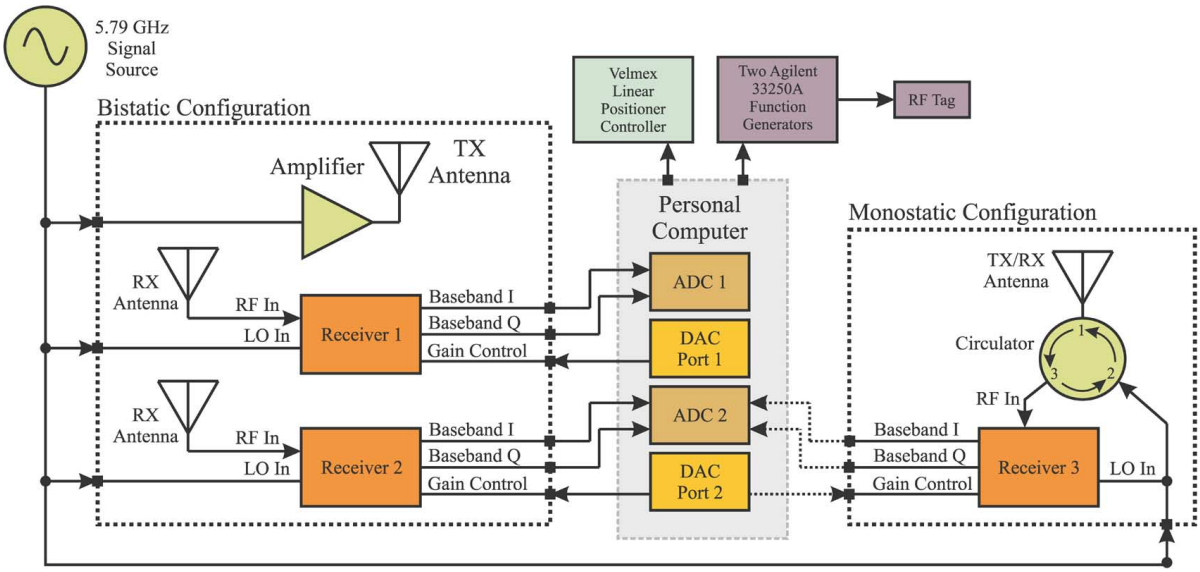

Fig. 1. The block diagram of the backscatter testbed designed and prototyped for microwave multipath measurements. The testbed consisted of laboratory test-and-measurement equipment as well as custom direct-conversion receivers and custom RF tags. The testbed can be configured for either monostatic or bistatic operation. Both configurations are shown (modified from [14]).

channel with statistically independent Rician-fading links [15], [16]. It can be expressed

$$f_{\mathbf{A}}(\alpha) = \frac{4}{\sigma_f^2\sigma_b^2}\exp[-K_b - K_f]\sum_{i=0}^{\infty}\sum_{l=0}^{\infty}\frac{1}{(i!)^2(l!)^2}\left(\frac{K_b}{\sigma_b^2}\right)^i \times \left(\frac{K_f}{\sigma_f^2}\right)^l\left(\frac{\sigma_b}{\sigma_f}\right)^{i-l}\alpha^{i+l+1}\mathrm{K}_{(i-l)}\left(\frac{2\alpha}{\sigma_b\sigma_f}\right) \quad (1)$$

where $\mathbf{A}$ is the random channel envelope; α is the index of the distribution; σ_f^2 and σ_b^2 are the envelope variances of the forward and backscatter links, respectively; K_f and K_b are the Rician K factors of the forward and backscatter links, respectively; and $\mathrm{K}_\nu(\cdot)$ is a modified bessel function of the second kind with order $\nu = i - l$. In (1), it is assumed that the reader transmitter, reader receiver, and RF tag antennas are adequately separated in space to decorrelate propagation paths in the forward and backscatter links—i.e., link correlation is equal to zero [10]. Expressions of the general $M \times L \times N$ backscatter channel envelope distribution with Rician-fading links have not been derived. See Section IV-C for discussion.

III. The Measurement Setup

A. The Backscatter Testbed and Measurement Setup

This section summarizes the custom testbed for the NLOS measurements discussed previously [14] and expands upon it to include details of the LOS measurements presented in this paper.

The testbed could be arranged in either a bistatic or monostatic configuration, as shown in Fig. 1 (modified from [14]). Three custom, linearly-polarized patch antennas each with a broadside gain of approximately 3.8 dBi were used in the testbed. The bistatic configuration employed one patch antenna to transmit and two to receive; however, in the monostatic configuration, a single patch antenna was used with a microwave circulator to transmit and receive. The transmitted continuous wave (CW) and receiver local oscillator (LO) signals were supplied by a single signal source to allow phase stable measurements. Three custom, coherent, direct-conversion receivers were used to down-convert the modulated backscatter signal received from the RF tag. The receiver for the monostatic configuration had a different front-end than the receivers used in the bistatic configuration allowing it to operate linearly while receiving strong transmitter-antenna reflections returning through the circulator. The baseband I and Q signals from each receiver were digitized and stored in a personal computer for off-line processing. Two custom RF tags were designed for the testbed. The first, the single-antenna tag (STAG), used a single antenna to modulate backscatter and the second, the dual-antenna tag (DTAG), used two antennas.

Multipath fading measurements were made with the testbed in its monostatic and bistatic configurations using both the single-antenna and dual-antenna tags for a total of four setup combinations. All four setups were measured under LOS conditions, while only the bistatic setups were used in NLOS conditions. NLOS measurements were not feasible for the monostatic setups because reflections from the transmitter antenna entered the receiver through the circulator limiting the reader's maximum transmit power. Therefore, the following six channels were measured: the LOS, monostatic single-antenna-tag channel; the LOS, monostatic dual-antenna-tag channel; the LOS, bistatic single-antenna-tag channel; the LOS, bistatic dual-antenna-tag channel; the NLOS, bistatic single-antenna-tag channel; and the NLOS, bistatic dual-antenna-tag channel.

The LOS measurements were conducted in room E560 (VLE560) of the Van Leer Building, shown in Fig. 2 (modified from [14]), on the Georgia Institute of Technology Atlanta campus. Although a strong LOS existed between the testbed

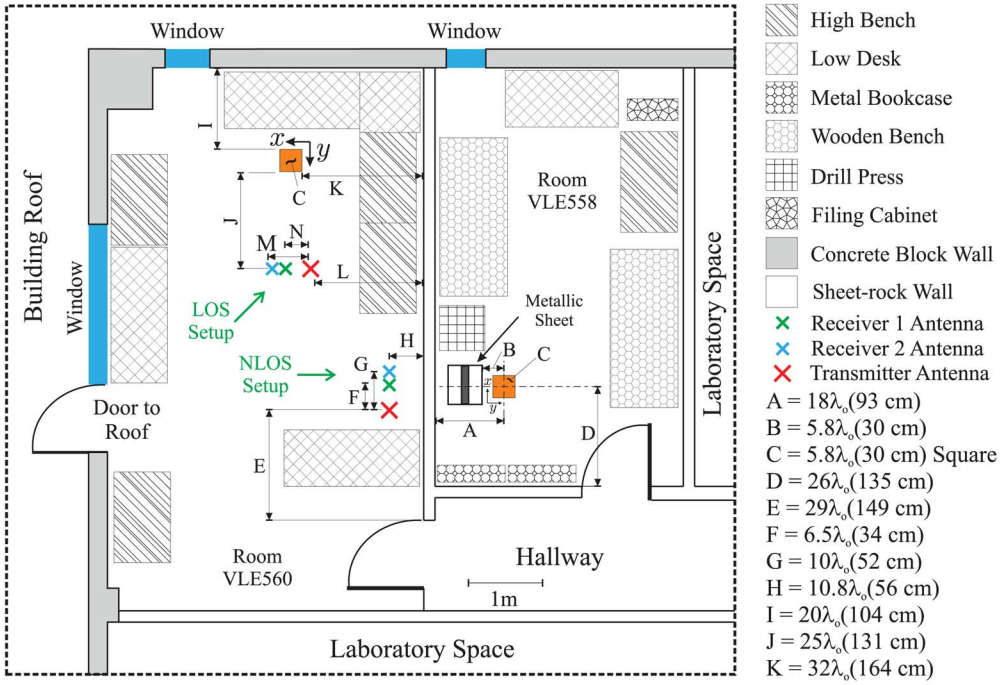

Note 1: The base of the metallic sheet (actually a stripline cavity) is 53cm x 46cm. The actual metallic stripline (shown in black) is 51cm x 10cm x 161cm.
Note 2: For the LOS monostatic setup (not shown), the transmitter/receiver antenna was located at L = $34\lambda_o$(179 cm) .

Fig. 2. The bistatic measurement setups for the LOS and NLOS measurements in rooms E560 and E558 of the Van Leer Building at Georgia Tech. Coherent channel samples were taken at 5.79 GHz as a function of RF-tag position (a sample was recorded every 1 cm or approximately every $\lambda_o/5$) across the square area with dimension C (modified from [14]).

reader and the RF tag, multipath propagation was still noticeable due to the walls, floor, and ceiling of the room; laboratory desks and workbenches; and other miscellaneous objects located in the laboratory. In these measurements, the RF tag and reader antennas were approximately 178 cm above the floor.

In contrast, the NLOS measurements were conducted with the reader transmitter and receiver located in room E560 of the Van Leer Building and the RF tag located in room E558 (VLE558), as shown in Fig. 2. The LOS was blocked by both a sheet-rock wall and a large metal sheet (i.e., the side of a stripline cavity). The RF tag and reader antennas were approximately 86 cm above the floor.

In all of the measurements, a 5.79 GHz, unmodulated carrier was transmitted from the reader and modulated by the RF tag with a 31-bit, maximal-length pseudo-random code (m-sequence) [17] at a chip rate of 1 MHz. To measure fading as a function of RF-tag position in an unbiased manner, channel measurements were taken with RF-tag positions distributed evenly over a square area, shown in Fig. 2. A screw-drive linear positioner moved the RF tag in 1 cm increments across a 30 cm $\times$ 30 cm square area. The testbed was calibrated before each measurement and all measurements are reported relative to their respective calibrations. Details of the calibration procedure and the testbed dynamic range and sensitivity are available in previously published work [14], [16].

B. Backscatter Signaling

The signal received from the RF tag is graphically depicted in Fig. 3(a). In a static channel, the modulated carrier is down-converted and the resulting baseband signal can be decomposed into a constant signal $\tilde{V}_{\text{avg}}$ and a time-varying signal $\tilde{V}_{\text{data}}$ that contains the information from the RF tag. Assuming that the RF-tag switches its reflection coefficient between two states for communication, $\tilde{S}_{\text{A}}$ and $\tilde{S}_{\text{B}}$, the signals can be represented on an IQ diagram as shown in Fig. 3(b). Here, the signal received by the reader in RF-tag impedance state A $\tilde{S}_{\text{A}}$ is the vector sum of the transmitted carrier (plus other smaller, unmodulated scattered signals) $\tilde{C}$ and the modulated-backscatter signal, which is proportional to the RF-tag antenna load reflection coefficient $\tilde{\Gamma}_{\text{A}}$. Likewise, the received signal in RF-tag impedance state B $\tilde{S}_{\text{B}}$ is the sum of $\tilde{C}$ and a signal proportional to $\tilde{\Gamma}_{\text{B}}$. The corresponding baseband equation for $\tilde{S}_{\text{A}}$ and $\tilde{S}_{\text{B}}$ can be written as

$$\tilde{S}_{\text{A}} = \frac{1}{2}\tilde{\text{h}}^b\tilde{\Gamma}_{\text{A}}\tilde{\text{h}}^f\tilde{x} \tag{2}$$

$$\tilde{S}_{\text{B}} = \frac{1}{2}\tilde{\text{h}}^b\tilde{\Gamma}_{\text{B}}\tilde{\text{h}}^f\tilde{x} \tag{3}$$

where $\tilde{\text{h}}^f$ and $\tilde{\text{h}}^b$ are the complex, baseband coefficients of the forward and backscatter links, respectively, and $\tilde{x}$ is the CW tone transmitted from the reader.[1] In terms of $\tilde{V}_{\text{avg}}$ and $\tilde{V}_{\text{data}}$, these equations become [19]

$$\tilde{S}_{\text{A}} = \tilde{V}_{\text{avg}} + \frac{1}{2}\tilde{V}_{\text{data}} \tag{4}$$

$$\tilde{S}_{\text{B}} = \tilde{V}_{\text{avg}} - \frac{1}{2}\tilde{V}_{\text{data}}. \tag{5}$$

[1]The 1/2 in (2) and (3) simply conserves power when the equations are converted to their passband representations [18].

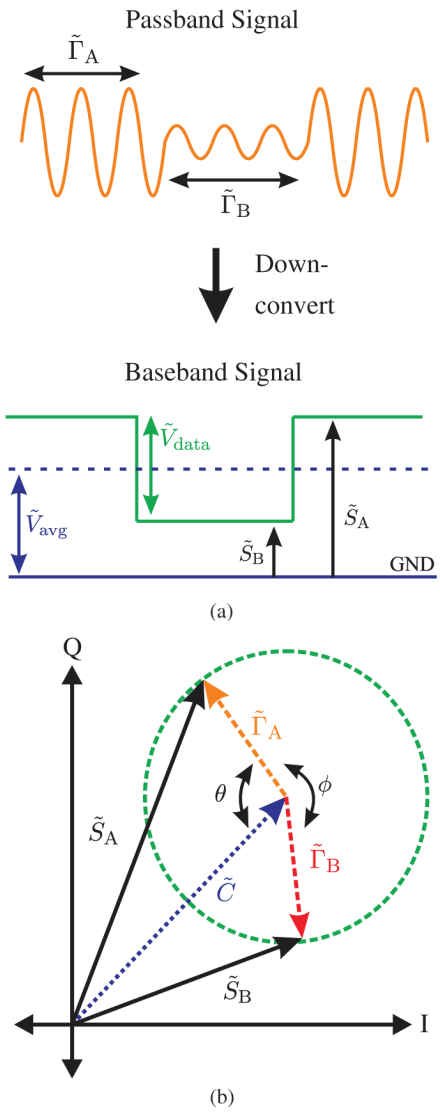

Fig. 3. (a) The passband and baseband signal received from a backscatter RF tag. (b) An IQ diagram showing the components of the backscatter signal received at the reader.

Or, after some manipulation, (2) and (3) can be written [19]

$$\tilde{V}_{\text{avg}} = \frac{\tilde{S}_A + \tilde{S}_B}{2} = \frac{1}{4}\tilde{h}^b\tilde{h}^f(\tilde{\Gamma}_A + \tilde{\Gamma}_B)\tilde{x} \quad (6)$$

$$\tilde{V}_{\text{data}} = \frac{\tilde{S}_A - \tilde{S}_B}{2} = \frac{1}{4}\tilde{h}^b\tilde{h}^f(\tilde{\Gamma}_A - \tilde{\Gamma}_B)\tilde{x}. \quad (7)$$

In the measurements reported in this paper, $\tilde{V}_{\text{avg}}$ was removed from the total received signal with a DC blocking capacitor and the envelope distribution estimates were calculated using $\tilde{V}_{\text{data}}$, which is proportional to the difference between the complex reflection coefficients.[2]

One interesting aspect of backscatter signaling is that, although the phase ϕ between $\tilde{\Gamma}_A$ and $\tilde{\Gamma}_B$ is fixed, as shown in Fig. 3(b), their phase θ relative to $\tilde{C}$ is not. This phase can change with the relative reader and RF-tag positions as well as with alterations in the RF-tag antenna impedance. Therefore, it is always possible that θ could change such that $\tilde{S}_A$ and $\tilde{S}_B$ have the same magnitude. In such a situation, an envelope receiver, which can only detect the magnitude of the signals, would not detect the difference between the modulation states; therefore, coherent receivers were used for these measurements.

IV. Measurement Results

A. NLOS Measurement Results

The NLOS measurements have been discussed in detail previously [14], but are summarized here for comparison with the LOS measurements. NLOS measurements with both the single-antenna tag and dual-antenna tag exhibited deep, rapid fades of up to 40 dB; however, fading in the dual-antenna tag measurement was less severe than that with the single-antenna tag. Thus, a pinhole diversity gain was observed. Furthermore, the measured distribution estimates closely matched the analytical product-Rayleigh distributions discussed previously [10].

B. LOS Measurement Results

1) LOS Spatial Fading Plots: Fig. 4 shows plots of the LOS fading measurements as a function of RF-tag position. Each plot is normalized by the maximum received power. As expected, these plots show much less severe fading than the NLOS measurements. The maximum fade for the bistatic LOS channel was approximately 13 dB while that for the monostatic LOS channel (not shown) was approximately 20 dB. Fading was caused by specular reflections from the concrete block wall behind the measurement area and metal work benches and laboratory equipment on either side. For reference, the largest power received in any of the the LOS bistatic or monostatic measurements was -56 dBm and -83 dBm, respectively.[3]

2) LOS Fading Distributions: Estimates of the fading CDFs in the LOS channel using the monostatic and bistatic reader configurations are shown in Fig. 5 for both the single-antenna and dual-antenna tags. All of the distribution plots in this paper are normalized by the square root of the average power of the distribution $\sqrt{P}$. The average power is defined as $P = \int_0^\infty \alpha^2 f_{\mathbf{A}}(\alpha)d\alpha$ where $f_{\mathbf{A}}(\alpha)$ is the envelope probability distribution function and α is the channel envelope.

For both types of RF tags in Fig. 5, fading in the monostatic channel is more severe than that of the bistatic. The reason for this difference is that using spatially-separated transmitter and receiver antennas at the reader reduces link correlation [10]. While Fig. 5 shows that the monostatic channel has a higher probability of a deep fade than the bistatic channel, it also shows that the monostatic channel has a higher probability of a large envelope. Therefore, large link correlation tends to make fading in the channel swing between extremes because it correlates both destructive interference (fades) and constructive interference (peaks).

The fade margins given in Table I, which were calculated from the measured single-antenna and dual-antenna tag CDF estimates, show that pinhole diversity gains do occur in the LOS

[2]The formulation of $\tilde{V}_{\text{data}}$ would be different if a reference other than the DC level had been chosen.

[3]Note that these absolute power values are not normalized by the calibration measurements.

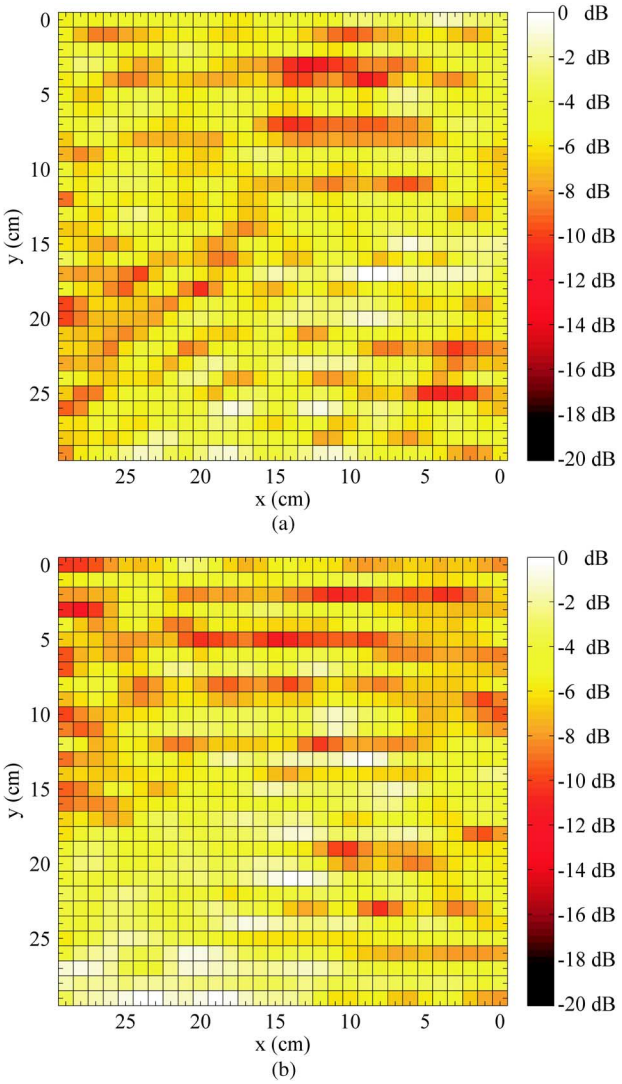

Fig. 4. Measured signal power (in dB) received from the (a) single-antenna and (b) dual-antenna tags in the LOS setup. The coloring of each square represents the modulated signal power received from the RF tag at each RF tag (x, y) position. The power is normalized by the maximum received and the orientation of the x and y axes is given by the LOS setup diagram shown in Fig. 2.

channel; however, they are very small. The fade margin is defined as [14]

$$\mathrm{FM} = 10\log_{10}\left[\frac{\left[F_{\mathbf{A}}^{-1}(\text{Outage Probability})\right]^2}{P}\right] \quad (8)$$

where $F_{\mathbf{A}}(\cdot)$ is the CDF and P is the average power of the distribution. The outage probability is the likelihood that the power received at the reader receiver P_{R} has faded below P by an amount equal to the fade margin—i.e., $\text{Outage Probability} = Pr[P_{\mathrm{R}} \leq P/(\mathrm{FM})]$ [14]. The measured monostatic and bistatic CDF estimates for the LOS channel are plotted in Fig. 6 and Fig. 7, respectively, along with the CDF calculated from (1). These figures show that the distribution estimates of the single-antenna and dual-antenna tags (for both the monostatic and bistatic reader configurations) approximate the $1 \times 1 \times 1$ product-Rician CDF calculated from (1).

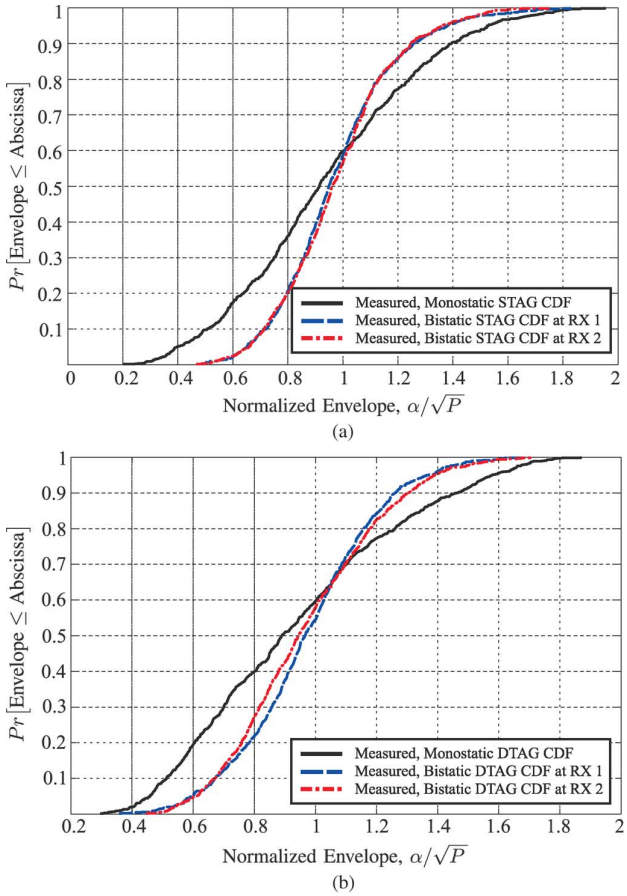

Fig. 5. Comparison of the monostatic and bistatic CDF estimates for the (a) single-antenna tag and (b) dual-antenna tag measurements in the LOS channel. The CDF estimates are plotted on axes normalized by the root of the power of each distribution $\sqrt{P}$ for unbiased comparisons.

C. Discussion

Several observations can be made from the LOS measurements outlined in the previous section. First, Fig. 5 indicates that using separate, adequately-spaced reader transmitter and receiver antennas decreases link correlation in the LOS backscatter channel and provides a corresponding reduction in multipath fading. Second, the estimate of the single-antenna tag CDF measured in the bistatic channel and the product-Rician distribution from (1) are a good match for $K_f = K_b = 13\,\mathrm{dB}$, shown in Fig. 7(a). Third, very small pinhole diversity gains are realized for the LOS channels using the monostatic and bistatic reader configurations as shown by the fade margins in Table I.

An unexpected result is that the measured estimates of the dual-antenna tag CDF at each receiver antenna, shown in Fig. 7(b), closely match the product-Rician CDF calculated from (1). One might expect that the strong specular waves scattered from each tag antenna would interfere and worsen the fading distribution compared to that of the single-antenna tag [16] or at least the distribution estimate measured with the dual-antenna tag would differ from that measured with the single-antenna tag. The similarity between the single-antenna and dual-antenna tag distributions can be explained by additional correlation in the LOS backscatter channel.

In the NLOS measurements, the high level of multipath propagation experienced by the RF tag resulted in a channel with

TABLE I
FADE MARGINS (IN dB) CALCULATED FROM THE MEASURED, LOS DISTRIBUTION ESTIMATES

Outage Probability	Monostatic		Bistatic	
	STAG	DTAG	STAG	DTAG
			RX 1 / RX 2	RX 1 / RX 2
0.5	0.78	1.0	0.47 / 0.36	0.31 / 0.50
0.1	5.9	5.8	2.9 / 2.9	3.5 / 3.5
0.05	8.0	6.8	3.7 / 3.6	4.6 / 4.4
0.01	10	8.9	5.7 / 5.5	6.5 / 5.7
0.005	11	9.9	6.0 / 5.9	7.7 / 6.3

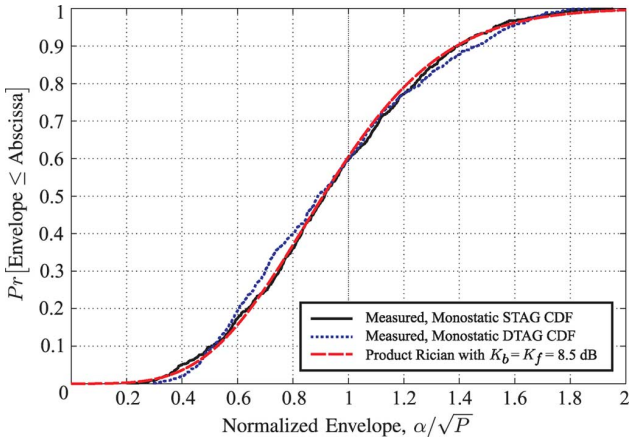

Fig. 6. The monostatic CDF estimates for the single-antenna tag and dual-antenna tag in the LOS channel along with the product-Rician CDF calculated from (1) for $K_f = K_b = 8.5$ dB. The CDF estimates are plotted on axes normalized by the root of the power of each distribution $\sqrt{P}$ for unbiased comparisons.

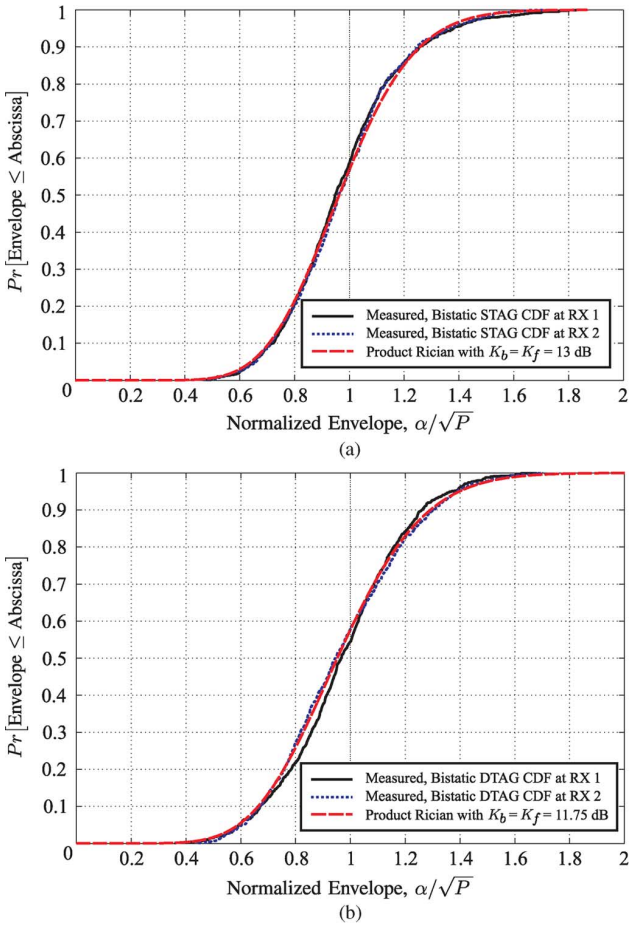

Fig. 7. The bistatic CDF estimates for the (a) single-antenna tag and (b) dual-antenna tag in the LOS channel along with the product-Rician CDF calculated from (1). The CDF estimates are plotted on axes normalized by the root of the power of each distribution $\sqrt{P}$ for unbiased comparisons.

a very small spatial coherence distance—i.e., the correlation of the channel as a function of space decreased rapidly [18]. Therefore, it can be assumed that signals received from each tag antenna had very low correlation. This assumption was confirmed by the close match between the measured NLOS distribution estimates and the previously derived analytical product-Rayleigh distributions, which assume that the signals received from each tag antenna are statistically independent [14]. The spatial coherence distance of the LOS channel, however, was much greater than that of the NLOS channel and resulted in correlation between the signals received from the two RF-tag antennas. In other words, the pinholes of the LOS backscatter channel were correlated and adding pinholes offered no additional statistically independent paths over which signals could propagate. In essence, a single phase front propagated from the tag to the reader which made the estimate of the dual-antenna tag distribution resemble that of the single-antenna tag. In a strong LOS channel, RF-tag footprint restrictions will likely not allow adequate antenna spacing to reduce this correlation; however, fading improvements can still be realized using widely separated receiver antennas, as shown in Fig. 5.

Since the signal backscattered from each RF-tag antenna is not independent, it is not possible to generalize (1) to the $M \times L \times N$ channel as was done with the product-Rayleigh distributions described previously [10]. Even so, the LOS measurements and the arguments above indicate (1) was adequate for tags with one and two antennas in very strong LOS channels.

It should be noted that the fading distribution estimates measured at 5.8 GHz are valid at other frequencies. The product-Rayleigh distributions [10] and product-Rician distribution given by (1) are valid in a local area—i.e., the area over which the channel can be accurately represented by a sum of planewaves arriving from the horizon [18]—at any frequency. While the choice of frequency certainly affects propagation characteristics, a local area experiencing some combination of non-specular and specular propagation in the 902–928 MHz band (a popular frequency band for RFID applications in the United States) will follow the same fading distribution as a local area with the same combination of non-specular and specular waves at 5.8 GHz. While the product-Rayleigh [10] and product-Rician distributions may not hold for every situation, they will apply when propagation in the local area of interest is similar to that of the environments measured in this paper. This is not overly restrictive and simply means that, for NLOS channels, propagation in the local area will be composed of a diffuse grouping of nonspecular waves. For LOS channels, local area propagation will be dominated by a single specular wave plus a diffuse group of nonspecular waves.

TABLE II
FADE MARGINS (IN dB) CALCULATED WITH AND WITHOUT MRC FROM THE MEASURED DISTRIBUTION ESTIMATES OF BOTH THE BISTATIC, NLOS CHANNEL AND THE BISTATIC, LOS CHANNEL

Outage Probability	NLOS Channel						LOS Channel					
	MRC		STAG†		DTAG†		MRC		STAG†		DTAG†	
	STAG	DTAG	RX 1	RX 2	RX 1	RX 2	STAG	DTAG	RX 1	RX 2	RX 1	RX 2
0.5	2.8	1.8	3.4	4.1	2.6	2.9	0.3	0.23	0.47	0.36	0.31	0.50
0.1	13	8.8	14	16	12	12	2.2	2.7	2.9	2.9	3.5	3.5
0.05	16	11	18	20	15	14	3.0	3.4	3.7	3.6	4.6	4.4
0.01	22	16	24	27	22	23	4.8	4.5	5.7	5.5	6.5	5.7
0.005	26	18	29	29	25	26	5.3	5.3	6.0	5.9	7.7	6.3

† No MRC performed.
The NLOS fade margins without MRC have been reported previously [14].

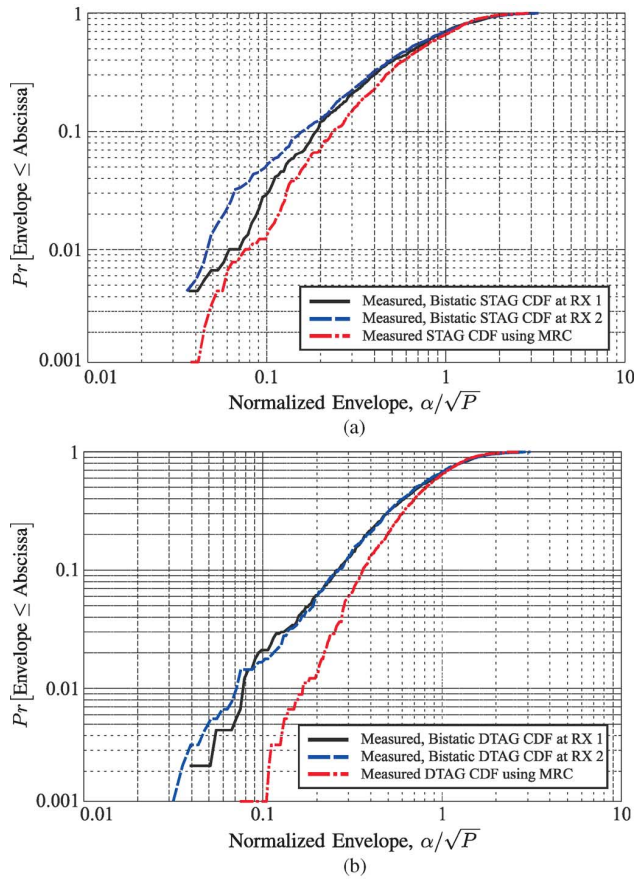

Fig. 8. Estimates of the bistatic, NLOS CDFs calculated using MRC compared to previous measurements [14] without MRC for the (a) single-antenna tag and (b) dual-antenna tag measurements. The CDFs are plotted on axes normalized by the root of the power of each distribution $\sqrt{P}$ for unbiased comparisons.

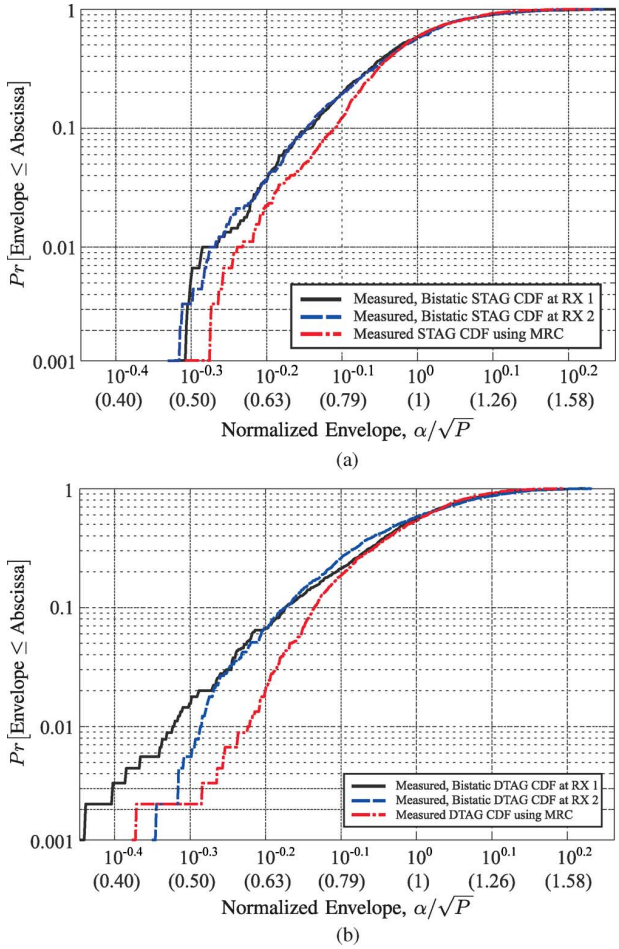

Fig. 9. Estimates of the bistatic, LOS CDFs with and without MRC for the (a) single-antenna tag and (b) dual-antenna tag measurements. The CDFs are plotted on axes normalized by the root of the power of each distribution $\sqrt{P}$ for unbiased comparisons.

D. Conventional Diversity Gains in the Backscatter Channel

Conventional diversity combining will also provide link gains in the backscatter channel. Maximal ratio combining (MRC) [18] was used to combine the signals received from the single-antenna and the dual-antenna tags in both the NLOS and LOS backscatter channels. The RF-tag reader was assumed to have perfect knowledge of the channel and results are compared to previous results without MRC [14] in terms of CDFs and fade margins in Figs. 8, 9 and Table II, respectively.

As shown in Fig. 8, MRC improved all the measured cases, with the most significant improvement observed for the NLOS channel measurements taken with the dual-antenna tag. The additional antennas of the dual-antenna tag added pinholes doubling the signal pathways in the multipath-rich environment.

V. CONCLUSION

The multipath fading measurements presented in this paper show that multipath fading exists in both the NLOS and LOS backscatter channels. Deep fades of up to 40 dB were observed on the signal backscattered from the RF tag in the NLOS

channel while much smaller (up to 20 dB) fades were measured in the LOS channel. Fading in the NLOS measurements followed a product-Rayleigh distribution while that of the LOS channel followed a product-Rician distribution. Multipath fading was reduced using multiple RF tag antennas—i.e., a pinhole diversity gain—in the NLOS channel, but only very small pinhole diversity gains were observed in the LOS channel. Even so, fading in both the NLOS and LOS channels was reduced by using a bistatic reader with widely-spaced transmitter and receiver antennas instead of a monostatic receiver. The benefits of using MRC at the reader receiver were calculated and showed that maximum diversity gains were realized in systems that used multiple RF tag antennas.

APPENDIX
LIST OF ACRONYMS

ADC	analog-to-digital converter.
CDF	cumulative distribution function.
CW	continuous wave.
DAC	digital-to-analog converter.
DTAG	dual-antenna tag.
LOS	line-of-sight.
STAG	single-antenna tag.
$M\times L\times N$	a backscatter channel with M transmitter,L RF tag, and N receiver antennas.
NLOS	non-line-of-sight.
MRC	maximal ratio combining.
RFID	radio frequency identification.

ACKNOWLEDGMENT

The authors would like give a special thanks to R. Pirkl for his expert hardware and data processing advice and J. Duvall for her assistance with the measurements.

REFERENCES

[1] Auto-ID Centre White Papers from Cambridge, U.K., "UHF band RFID readability and fading measurements in practical propagation environment," 2005, pp. 37–44.
[2] J. Mitsugi and Y. Shibao, "Multipath identification using steepest gradient method for dynamic inventory in UHF RFID," presented at the Int. Symp. on Applications and the Internet, SAINT Workshops, Hiroshima, Japan, 2007.
[3] M. Polivka, M. Svanda, and P. Hudec, "Analysis and measurement of the RFID system adapted for identification of moving objects," in *Proc. 36th Eur. Microwave Conf.*, Sep. 2006, pp. 729–732.
[4] L. W. Mayer, M. Wrulich, and S. Caban, "Measurements and channel modeling for short range indoor UHF applications," in *Proc. 1st IEEE Eur. Conf. on Antennas Propag. EuCAP 2006*, Nov. 2006, pp. 1–5.
[5] U. Muehlmann, G. Manzi, G. Wiednig, and M. Buchmann, "Modeling and performance characterization of UHF RFID portal applications," *IEEE Trans. Microw. Theory Tech.*, vol. 57, no. 7, pp. 1700–1706, 2009.
[6] A. Lazaro, D. Girbau, and D. Salinas, "Radio link budgets for UHF RFID on multipath environments," *IEEE Trans. Antennas Propag.*, vol. 57, no. 4, pp. 1241–1251, 2009.
[7] S. R. Banerjee, R. Jesme, and R. A. Sainati, "Performance analysis of short range UHF propagation as applicable to passive RFID," in *Proc. IEEE Int. Conf. on RFID*, Grapevine, TX, Mar. 2007, pp. 30–36.
[8] S. R. Banerjee, R. Jesme, and R. A. Sainati, "Investigation of spatial and frequency diversity for long range UHF RFID," in *Proc. IEEE Antennas Propag. Society Int. Symp.*, San Diego, CA, Jul. 2008, pp. 1–4.
[9] D. Kim, M. A. Ingram, and W. W. Smith, Jr., "Measurements of small-scale fading and path loss for long range RF tags," *IEEE Trans. Antennas Propag.*, vol. 51, no. 8, pp. 1740–1749, Aug. 2003.
[10] J. D. Griffin and G. D. Durgin, "Gains for RF tags using multiple antennas," *IEEE Trans. Antennas Propag.*, vol. 56, no. 2, pp. 563–570, 2008.
[11] M. A. Ingram, M. F. Demirkol, and D. Kim, "Transmit diversity and spatial multiplexing for RF links using modulated backscatter," presented at the Int. Symp. on Signals, Systems, and Electronics, Tokyo, Jul. 24–27, 2001.
[12] J. S. Kim, K. H. Shin, S. M. Park, W. K. Choi, and N. S. Seong, "Polarization and space diversity antenna using inverted-F antennas for RFID reader applications," *IEEE Antennas Wireless Propag. Lett.*, vol. 5, no. 1, pp. 265–268, Dec. 2006.
[13] A. Rahmati, Z. Lin, M. Hiltunen, and R. Jana, "Reliability techniques for RFID-based object tracking applications," in *Proc. 37th Annu. IEEE/IFIP Int. Conf. on Dependable Systems and Networks (DSN'07)*, Edinburgh, U.K., Jun. 2007, pp. 113–118.
[14] J. D. Griffin and G. D. Durgin, "Multipath fading measurements for multi-antenna backscatter RFID at 5.8 GHz," in *Proc. Int. IEEE Conf. on RFID*, Orlando, FL, Apr. 2009, pp. 322–329.
[15] M. K. Simon, *Probability Distributions Involving Gaussian Random Variables: A Handbook for Engineers and Scientists*. Norwell, MA: Kluwer Academic Publishers, 2002.
[16] J. D. Griffin, "High-frequency modulated backscatter communication using multiple antennas" Ph.D. dissertation, The Georgia Institute of Technology, Atlanta, 2009.
[17] R. W. Dixon, *Spread Spectrum Systems With Commercial Applications*, 3rd ed. New York: Wiley Interscience, 1994.
[18] G. D. Durgin, *Space-Time Wireless Channels*. Upper Saddle River, NJ: Prentice Hall, 2003.
[19] J. T. Prothro and G. D. Durgin, "Improved performance of a radio frequency identification tag antenna on a metal ground plane" Master's thesis, The Georgia Institute of Technology, Atlanta, 2007.

Joshua D. Griffin received the B.S. degree in engineering from LeTourneau University, Longview, TX, in 2003, and the MSECE and Ph.D. degrees from the Georgia Institute of Technology (Georgia Tech), Atlanta, in 2005 and 2009, respectively.

In 2004, he joined the Propagation Group at Georgia Tech where he researched UHF and microwave propagation for backscatter radio. In 2006, he participated in a research exchange program with the Sampei Laboratory at Osaka University, Osaka, Japan. He joined the Radio and Antennas Group at Disney Research, Pittsburgh, PA, in 2009. His research interests include radio wave propagation, radiolocation, applied electromagnetics, backscatter radio, and radio frequency identification (RFID).

Dr. Griffin received the Graduate Research Assistant Excellence Award from the Electrical and Computer Engineering Department at Georgia Tech in 2009.

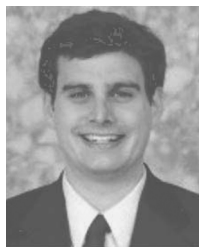

Gregory D. Durgin received the BSEE, MSEE, and Ph.D. degrees from Virginia Polytechnic Institute and State University, Blacksburg, in 1996, 1998, and 2000, respectively.

He is an Associate Professor in the School of Electrical and Computer Engineering, Georgia Institute of Technology, Atlanta, having joined the faculty in 2003. He spent one year as a Visiting Researcher with the Morinaga Laboratory at Osaka University, Osaka, Japan. He founded the Propagation Group (http://www.propagation.gatech.edu) at Georgia Tech, a research group that studies radiolocation, channel sounding, direction finding, backscatter radio, RFID, and applied electromagnetics. He is an active consultant to industry. He authored *Space-Time Wireless Channels*, the first textbook in the field of space-time channel modeling.

Prof. Durgin is a winner of the NSF CAREER Award as well as numerous teaching awards, including the Class of 1940 Howard Ector Outstanding Classroom Teacher Award (2007), and the 2001 Japanese Society for the Promotion of Science (JSPS) Postdoctoral Fellowship. In 1998, he was co-recipient of the Stephen O. Rice prize for best original journal article in the IEEE TRANSACTIONS ON COMMUNICATIONS.